

SIMULATION OF STRONG MOTION DURING THE 1995 HYOGO-KEN-NANBU EARTHQUAKE BY USING THE 2D/3D PSEUDOSPECTRAL METHOD

S HIGASHI¹

SUMMARY

A 2D/3D pseudospectral method for wave propagation is used for simulating the ground motions during the 1995 Hyogo-ken Nanbu earthquake in order to investigate the physical process of generating heavily damaged zone along the basin edge of the Kobe area. 2D P-SV wave field is calculated for three profile lines, the Juniken-road line, the Ikuta River - Port Island line, and the Takatori line, with detailed gradient underground structure in the Kobe area. The results show a clear constructive interference of the direct S-wave and diffracted/surface waves generated at the basin edge. The strong-motion distribution on the ground surface at each line is in good agreement with the observed damaged zone. The results of the 3D calculation show that the shape of the sediment/basement boundary significantly affects the wave field in the basin. In addition to the interference of the waves, convergence and divergence of the wave front occurred along the sediment/basement boundary. Additional parallel computing trial is carried out for the 3D calculation. The results show the efficiency in 3D pseudospectral calculation.

INTRODUCTION

Recent studies on the physical process of generating the heavily damaged zone in Kobe City caused by the 1995 Hyogo-ken Nanbu earthquake have shown that the effect of the basin edge is an important factor. There is general agreement in seismologists that the constructive interference between the direct S-wave and the diffracted/surface waves generated at the basin edge caused the damage belt in the Kobe area. This effect results from the irregular interface between sedimentary layer and basement rock. It can not be explained by laterally layered media. In this study, we will evaluate the effect of 2D/3D irregularity of the interface on seismic motion by using a staggered-grid pseudospectral method (Higashi and Sato, 1996). In 2D modeling, P-SV wave field is calculated using detailed gradient models along three seismic profiles, which have different interface shapes. In 3D modeling, we evaluate the effects of source rupture and 3D topography of the sediment/basement interface on the strong motions in the Kobe area.

2D MODELING

In this section, we investigate the physical process of generating the damage belt by using the detailed 2D model derived from the geophysical surveys. Figure 1 shows the damaged zone in the Kobe area (JMA seismic intensity of VII), three profile lines for 2D calculation, and the area for 3D calculation. During the main shock, strong-motion records were observed at those sites in the figure. KBU (Kobe University) is located on the Rokko granite.

The 2D models are based on the P-wave seismic reflection surveys, while the S-wave velocity and density are determined from the relations derived from the deep logging data (Matsumoto et al., 1998). Q-values are given corresponding to the S-wave velocity. These properties are given on the grids with a spacing of 25 m, so that the models have gradient properties. The lowest S-wave velocity is 270 m/s, while the P-wave and S-wave velocities

¹ *Geotechnical & Earthquake Engineering Dept, Ctl' Research Inst of Electric Power Ind. Email: higashi@criepi.denken.or.jp*

are 5000 m/s and 2500 m/s, respectively.

We calculate P-SV wave field by using the 2D pseudospectral method. Herrmann's pseudo-delta function with a time width of 0.4 s is incident vertically on the bottom of the models as a SV-wave. The number of grids for the models are 512*128. We apply absorbing boundary conditions (Cerjan et al., 1985) and a mapping method in order to reduce the wraparound at the artificial boundaries. The free surface conditions are introduced by using the symmetric displacement field and the antisymmetric stress field in order to avoid Gibbs phenomena at the free surface. The accurate frequency range is up to 5 Hz in the lowest velocity regions of 270 m/s at a spacing of 25 m. The calculation was run for 20000 time steps with a time spacing of 0.001 s (20 s) and required 5.8 hours on a DEC Alpha 500MHz workstation.

From the ground response for the pseudo-delta function, we calculate a frequency-domain response function at each grid on the ground relative to the rock outcrop of the Rokko granite side. The synthetic waveforms are obtained by convolving the observed records at KBU as a reference rock site. Figure 2 shows the calculated peak ground accelerations (PGA) and peak ground velocities (PGV), and the S-wave velocity models along the three profile lines. At the Juniken-road and Takatori lines, peaks of the distribution in PGA and PGV appear in the basin side offset 500 m from the basin edge, with the amplitudes of more than 1000 cm/s and 150 cm/s, respectively. Those amplified regions are in good agreement with the area of JMA seismic intensity of VII derived from Chuo Kaihatsu (1996). The distribution of PGV is smoother than that of PGA, but it corresponds to the observed damaged zone better. On the other hand, at the Ikuta River - Port Island line, two major peaks appear in the PGA and PGV distribution corresponding to the two edges on the basin interface. Those amplitudes are, however, smaller than those at the other lines, and the observed seismic intensity is also up to VI.

Snapshots of the SV-wave field at Juniken-road line are shown in Figure 3 for every 0.4 s from $t=1.2$ s to $t=3.6$ s. Just after the incidence of the S-wave with a positive amplitude on the sedimentary basin at $t=1.2$ s, a diffracted wave with a negative large amplitude generates at the bottom edge of the basin. The strong diffracted wave with a negative amplitude follows the direct S-wave along the basin edge ($t=1.6$ s and $t=2.0$ s). At the rock side, the incident S-wave hits the rock surface at 1.2 s and the surface wave generates and starts to propagate into the basin. The surface wave meets with the direct S-wave on the surface 500 m far from the basin edge. The diffracted wave hits the surface just after they met ($t=2.4$ s). The peak-to-peak amplitude at around this point becomes extremely larger than the other points. The amplitude variation of the ground motion is mainly attribute to the interference of these waves.

3D MODELING

Figure 1 shows the area modeled for 3D calculation. A 3D velocity model of the Kobe area derived by Miyakoshi et al.(1997), except for the uppermost layer of $V_s=350$ m/s, is used as a basic model. Furthermore, we modify the bedrock topography of their model by using a detailed contour map of the basement derived from the reflection survey and deep borehole loggings (Sano, 1998) since the basic model is too smooth to represent the complexity of the basin edge along the Kobe area. The south-western part of the model is partly extrapolated from the south-western boundary of the Sano's model in order to avoid artificial diffracted waves from a gap between both models. The topography above the sea level is not included. The velocity model deeper than 3 km is assumed to be laterally layered media and the velocity of each layer is the same as that used in the source inversion of Sekiguchi et al.(1998). Figure 4 shows the 3D model. Rock and soil properties of the model are shown in Table 1. The model has two sedimentary layers with the S-wave velocity of 550 m/s and 1000 m/s.

Complex source parameters of Sekiguchi et al.(1998) are used in this study. The fault plane consists of five segments, and the grid spacing of the point sources is 2.05 km. The most western segment located beneath Awaji Island is not included in our model because of the limitation of the 3D calculation. The segment does not contribute to the strong motion in the Kobe area very much since it is far from Kobe and the rupture goes backwards.

The 3D model is discretized with a grid spacing of 0.2 km. The dimension of the model is 25.6km(N320E)*51.2km(N050E)*25.6km(Z), so the number of the grids are 128*256*128. The absorbing boundary and free surface conditions are the same as 2D case. The moment-tensor source description for the staggered-grid parameterization (Graves, 1996) is used in this modeling. The moment-tensor components are represented as the distribution of equivalent body-force couples in this system. The accurate frequency range is up to 1.375 Hz in the lowest velocity regions of the model (0.55 km/s). The calculation was run for 3125 time steps with a time spacing of 0.008 s, that is, 25 s duration from the origin time, and required 55 hours on a DEC

Alpha 500MHz workstation.

Figure 5 shows the comparison of the simulated velocity waveforms (thin lines) with the filtered (0.1 - 2.0 Hz) observed velocity waveforms (thick lines) at the sites shown in Figure 1. The fault-normal (N320E), fault-parallel (N050E), and vertical (UP) components of the waveforms are shown in the figure. The lateral components of the synthetics at KBU and MOT are in good agreement with the observed data. There are, however, some differences in the vertical components at these sites. The first arrivals of the observed data are faster than those of the synthetics. At MOT, which is located on the sedimentary layer near the basin edge, the simulated peak ground velocity of the vertical component is much larger than the observed one. At FKA, PIS, and JMA, which are located in the western part of the Kobe area, the amplitudes of the first arrivals in the simulated fault-normal components can not reproduce those of the observed data. They are underestimated in the calculation. At JMA located on the sedimentary layer near the basin edge like MOT, the vertical component of the simulated velocity waveform also has a later arrival with a large amplitude. These results show that it is necessary to improve our 3D basin model.

Figure 6 shows the snapshots of the fault-normal component of ground velocity for the 3D simulation. These snapshots clearly demonstrate the effects of fault rupture and basin edge on the strong motion. Energy of seismic waves converges into the wave front in the forward direction of the fault rupture. After the wave front passes the basement side of the sediment/basement boundary, the wave front with a larger amplitude than that in the basement region propagates slowly in the sediment. The wave field in the Kobe area becomes complex due to the basin generated surface and diffracted waves. It is noteworthy that the later wave fronts generate along the sediment/basement boundary. Convergence and divergence of the wave fronts occur in the central part of the sediment ($T=11$ s). For later times ($t=15$ and 16 s), the wave field in the sediment remains due to basin generated waves, while the wave field in the basement rock has already vanished.

PARALLEL 3D PSEUDOSPECTRAL COMPUTATION

Recently, parallel 3D pseudospectral computing has been carried out for a large scale modeling (Furumura et al., 1995). Parallel operation in the 3D pseudospectral method will produce a fairly good speed up compared with conventional computation on a single processor. We modified our code using a MPI (Message Passing Interface) library on HITACHI SR2201 (64 PU). Each processor has a peak computing rate of 0.3 GFLOPS with a local memory of 256 Mbytes at an interprocessor communication rate of 300 Mbytes/s. As space is limited, we will only show the results of our experimental performance tests for the 3D model (256*128*128 grid points) described in the previous section. Figure 7 shows the ratio of computational speed and the amount of required memory for each processor with a number of processors to that for 4 processors. Although the speed-up rate for 64 processors becomes slower than the theoretical one, the maximum speed for SR2201 was 8 times faster than that for DEC Alpha mentioned before. The results show the efficiency of the parallel computing in 3D pseudospectral method.

DISCUSSION AND CONCLUSIONS

The results of the 2D pseudospectral calculation at three lines for the 1995 Hyogo-ken Nanbu earthquake showed a significant basin edge effect. The strong-motion distribution on the ground surface at each line was in good agreement with the observed damaged zone. From the snapshots for 2D wave field, we could see a clear constructive interference of the direct S-wave that propagates upward with the surface waves generated at the basin edge and the diffracted wave generated at the bottom edge of the basin. In 3D calculation, we evaluated strong motions at the observation sites. The results showed that the synthetic waveforms at KBU, a rock site, are in good agreement with the observation, whereas those at other sites in the sediment showed some differences in amplitude. The shape of the sediment/basement boundary significantly affects the wave field in the sediment. In addition to the constructive interference in the sediment observed in the 2D calculation, convergence and divergence of the wave front occurred along the sediment/basement boundary. The trial of the parallel pseudospectral computation developed efficiency in 3D calculation.

REFERENCES

Cerjan, C., Kosloff, D., Kosloff, R., and Reshef, M. (1985), A nonreflecting boundary condition for discrete acoustic and elastic wave equations, *Geophysics*, 50, 705-708.

Chuo Kaihatsu Corp. (1996), Final Report of Disaster Survey during the 1995 Hyogo-ken Nanbu Earthquake (in Japanese).

Furumura, T., Kennet, B. L. N., and Takenaka, H. (1998), Parallel 3-D pseudospectral simulation of seismic wave propagation, *Geophysics*, 63, 279-288.

Graves, R. W. (1996), Simulating seismic wave propagation in 3D elastic media using staggered grid finite differences, *Bull. Seism. Soc. Am.*, 86, 1091-1106.

Matsumoto, M., Koike, A., Yamada, M., Ito, Y., Iwasaki, Y., Yokota, H., Ito, S. (1998), Elastic properties of Osaka Group in the deep underground, *Proc. 98th SEGJ* (in Japanese).

Miyakoshi, K., Kagawa, T., and Echigo, T. (1997), Deep sedimentary structure model beneath the Osaka plain, *Proc. 96th SEGJ* (in Japanese).

Sano, M. (1998), Geological structure and concealed active faults of the Osaka Basin, *Proc. 11th Seminar of FRED-C*, 6-23 (in Japanese).

Sekiguchi, H., Irikura, K., and Iwata, T. (1998), Detailed source process of the 1995 Hyogo-ken Nanbu (Kobe) earthquake using near-field strong ground motion data, *Proc. 10th Japan Earthq. Eng. Symposium, STS-2*, #67.

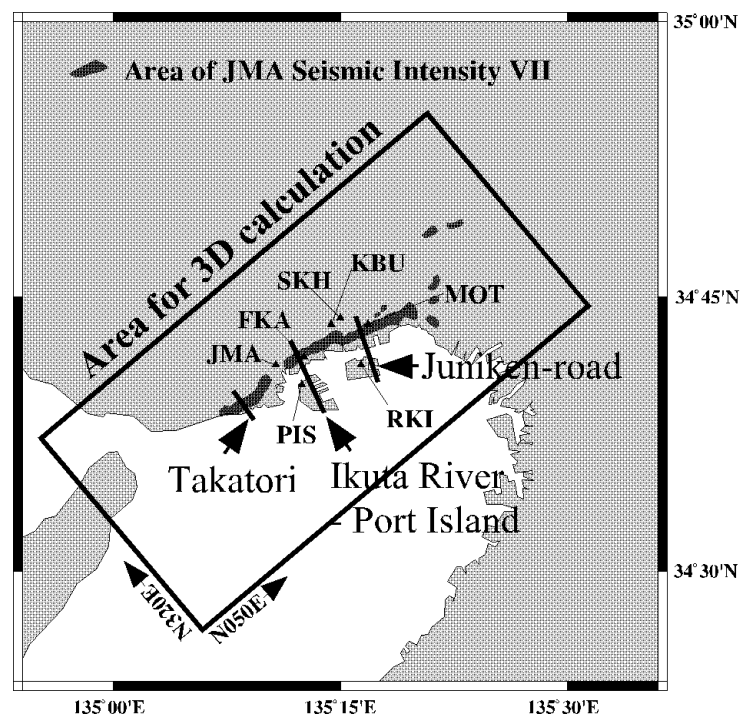


Figure 1: Location map of the lines for 2D calculation, the area for 3D calculation, and strong-motion recording sites in the Kobe area.

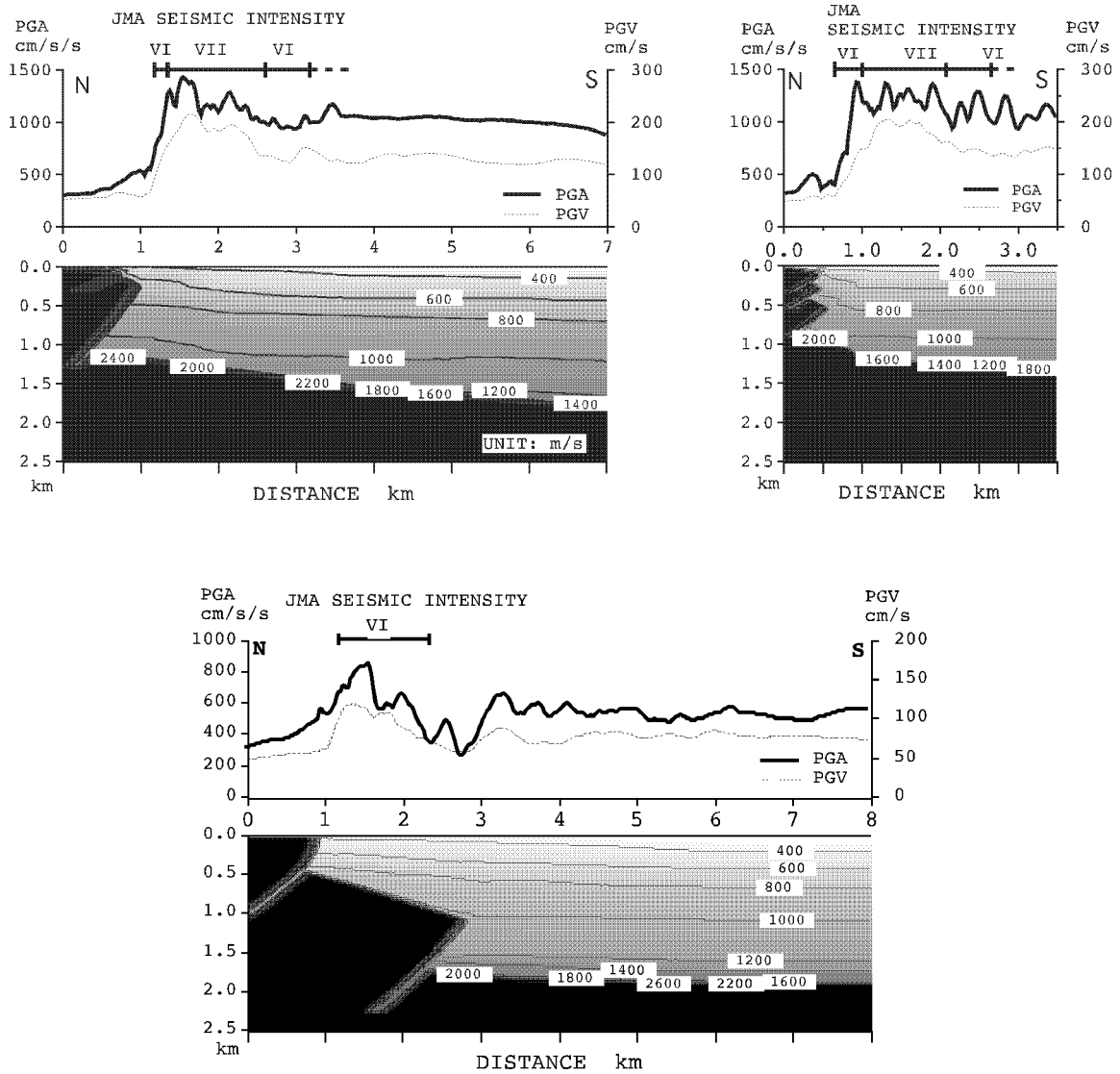


Figure 2: Peak ground acceleration (PGA) and peak ground velocity (PGV) along the profile lines (top left: Juniken-road ; top right: Takatori; and bottom: Ikuta River – Port Island). S-wave velocity models are shown below.

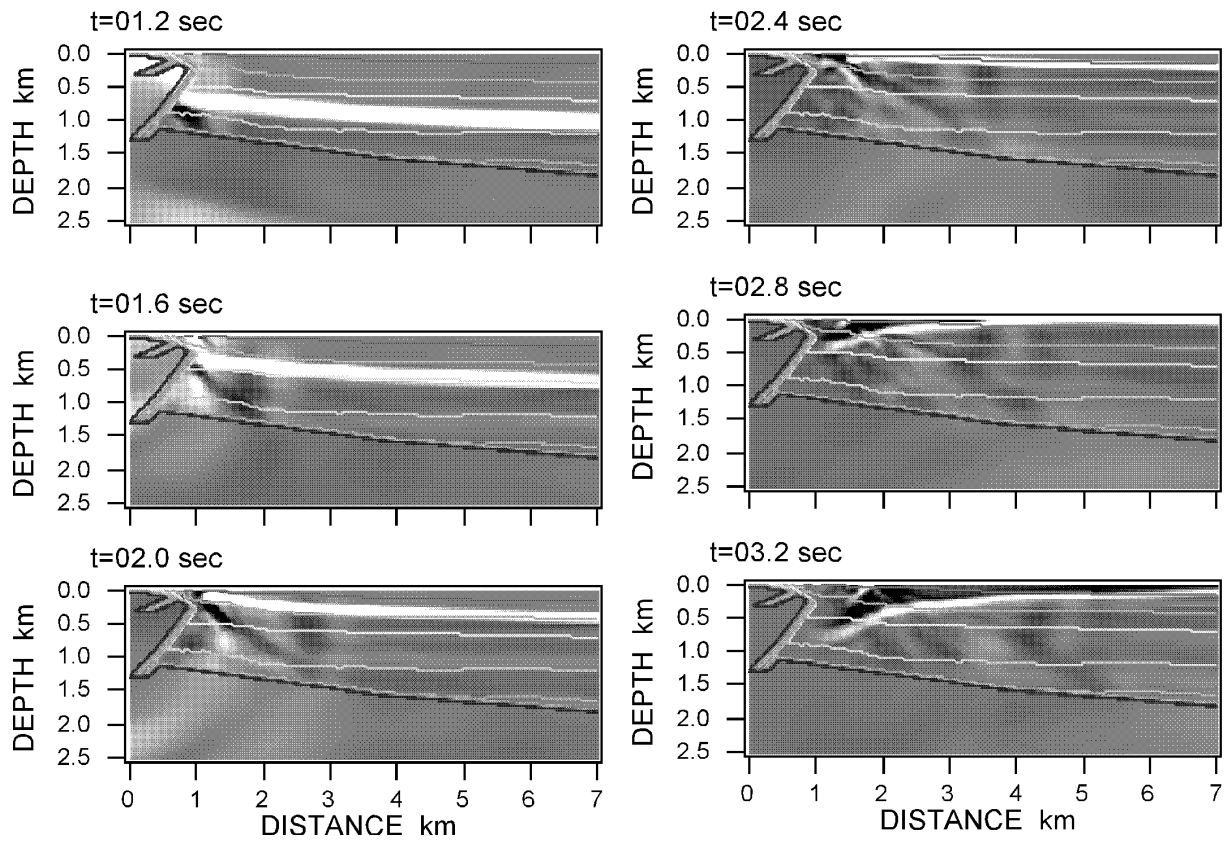


Figure 3: Snapshots of the P-SV wave field (horizontal component) at the Juniken-road line.

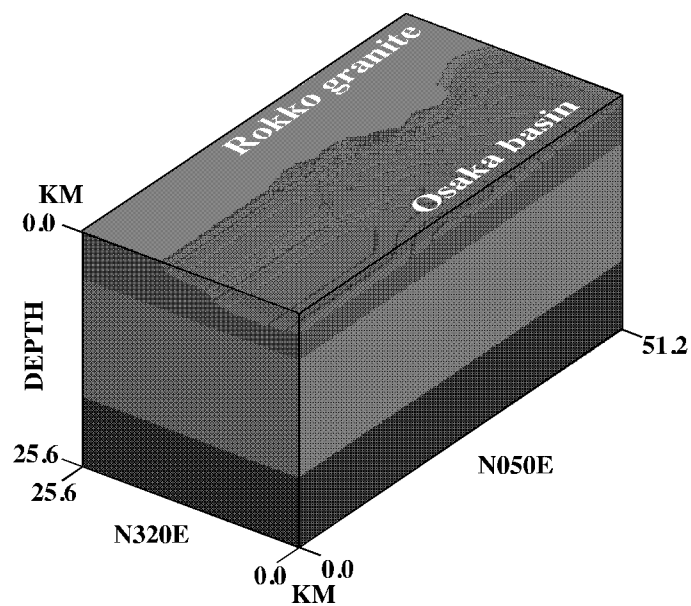


Figure 4: Bedrock topography in the Kobe area used in the 3D modeling.

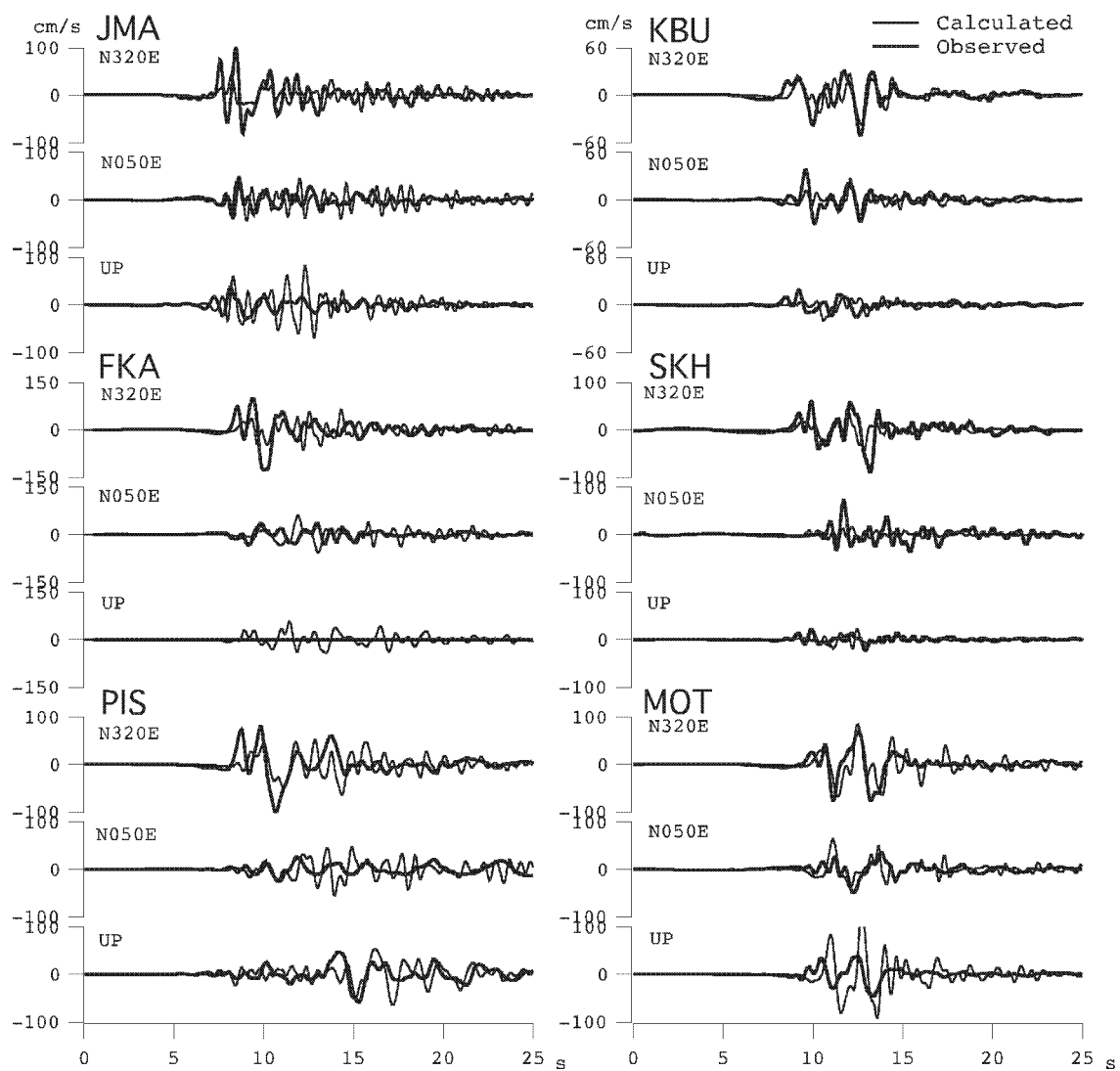


Figure 5: Comparison of the simulated velocity waveforms (thin lines) with the filtered (0.1-2.0 Hz) observed velocity waveforms (thick lines).

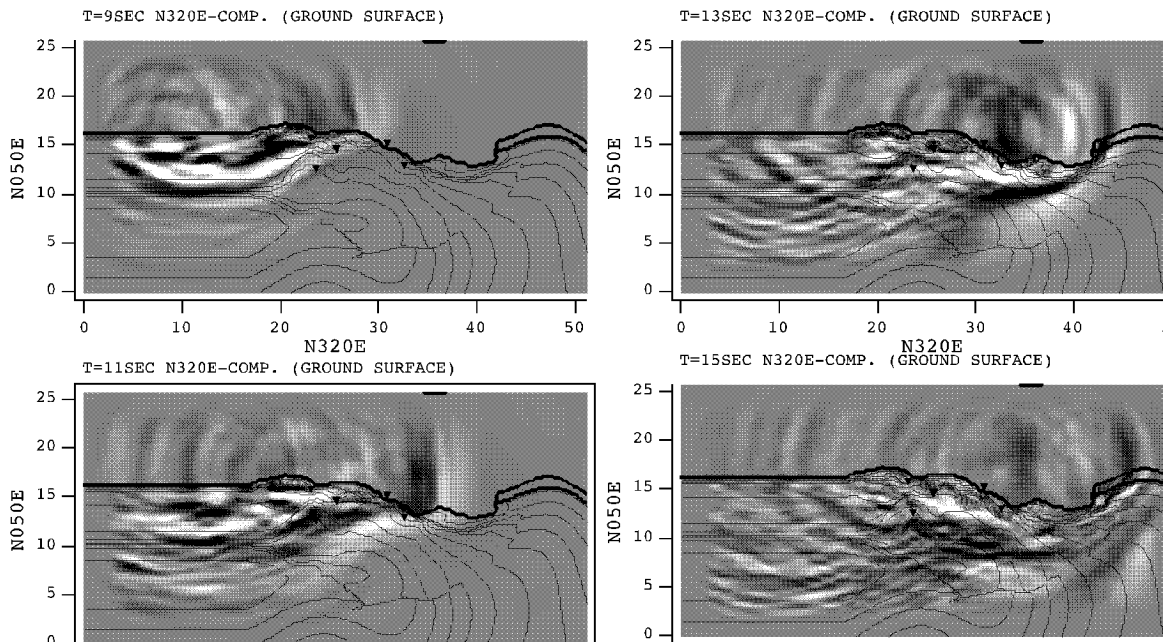


Figure 6: Snapshots of the fault-normal component of ground velocity for the 3D calculation.

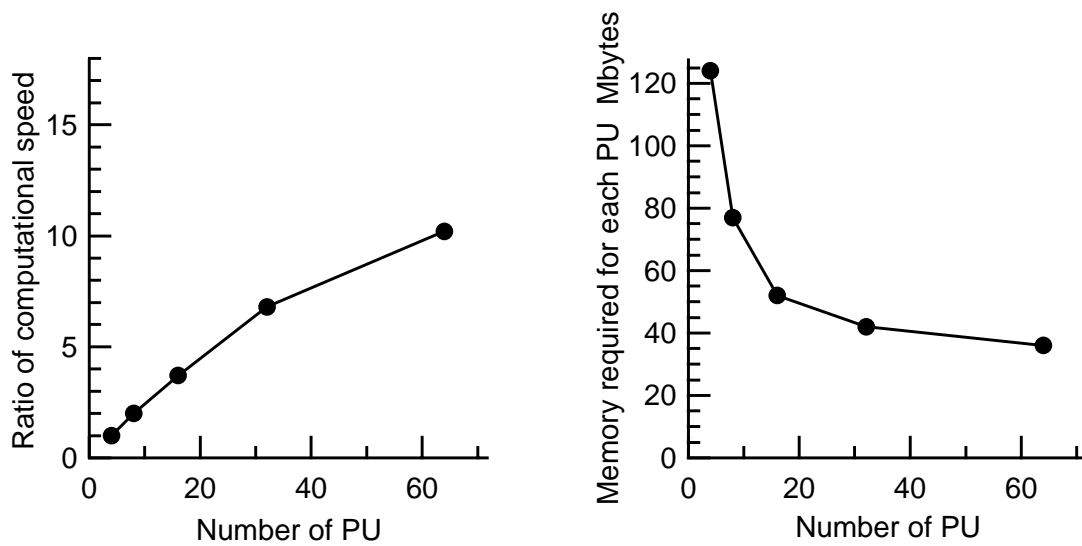


Figure 7: Ratio of computational speed and the amount of required memory for each processor plotted against the number of processors on HITACHI SR2201.